Subphase exploration for $SmFe_{12}$-based permanent magnets by Gibbs energies obtained with first-principles cluster-expansion method

Satoru Enomoto[a], Sonju Kou[a,1], Taichi Abe[b], Yoshihiro Gohda[a,*]

[a] *Department of Materials Science and Engineering, Tokyo Institute of Technology, Yokohama 226-8502, Japan*
[b] *National Institute for Materials Science, Tsukuba 305-0047, Japan*

Abstract

In the development of $SmFe_{12}$-based rare-earth permanent magnets, it is yet to establish a pathway to liquid-phase sintering producing nonmagnetic grain-boundary subphases. Here, phase equilibria of the Sm-Fe-Cu ternary system are examined computationally to explore such a pathway and grain-boundary subphases of $SmFe_{12}$-based magnets through Gibbs free energies for various phases. A key quantity, the mixing enthalpy is examined from first principles. We show that the B2 Sm-Cu-Fe is a candidate for a nonmagnetic subphase, where the solubility of Fe into Sm-Cu is better described by the cluster-expansion method finding attractive Cu-Fe interaction within the B2 sublattice. In addition, it is found that the liquid phase of Sm-Cu slightly including Fe directly equilibrates with $SmFe_{12}$, which is consistent with experiments. We point out the possibility of liquid-phase sintering of the $SmFe_{12}$-based magnets using this liquid phase without significant composition changes by the solidification. The mechanism of attractive interaction between Fe and Cu in B2 Sm(Cu, Fe) is clarified from the viewpoint of electron theory.

Keywords: Permanent magnets; Phase diagrams; Cluster-expansion method; First-principles electron theory; Materials Design

1. Introduction

As attempts to develop new rare-earth permanent magnets beyond $Nd_2Fe_{14}B$-based magnets, $SmFe_{12}$ have been studied intensively [1–16]. Even though magnetic properties such as the magnetization and the anisotropy field of $SmFe_{12}$ are superior to those of $Nd_2Fe_{14}B$, insufficient structural stability has been one of the most severe problems, which has been becoming gradually overcome as discussed below [6–9]. However, the design of $SmFe_{12}$-based magnets also suffers from identifying an appropriate grain-boundary subphase, a crucial component of microstructures. As an additive element for the grain-boundary phase, a few elements including Cu have been studied [15, 16]. In particular, it has been demonstrated that $SmFe_{11}Ti$ equilibrates with Cu-41at.% Sm at 1273 K [16]. Even though this finding is promising, phase equilibria for a wide temperature range are yet to be obtained. Such information should be helpful to design the sintering process of magnets. In addition, details of atomic interactions and atomic structures within the subphase are expected to be helpful for further optimization of microstructures.

Since $SmFe_{12}$ is a metastable phase in the Sm-Fe binary system, it must be stabilized by adding various elements such as Ti, V, Mo, Al, and Ga through Fe-site substitutions, and Zr, Y, and Gd for substituting Sm sites [9, 17–21]. Although Ti is an effective element to stabilize the compound, the processing temperature is higher than 1273 K [22, 23]. From the viewpoint of the liquid-phase sintering to achieve optimum microstructures, it requires the two-phase equilibria between the $SmFe_{12}$ and liquid phases. The two-phase equilibria are interrupted by the formation of other compounds in ternary and binary sub-systems, e.g., Fe_2Ti in the Fe-Ti binary system. Due to the Fe_2Ti precipitations, $SmFe_{12}$ does not have direct tie-lines to the liquid phase [16, 22, 23]. Among additive elements, Ti, Mo, and Zr have binary compounds with Fe, while V, Al and Cu are free from such compounds in the Fe-rich region of the binary phase diagram. As fundamental knowledge, it is of importance to examine if $SmFe_{12}$ can be in equilibrium with the liquid phase in ternary phase diagrams such as Sm-Fe-Cu, before proceeding to multicomponent phase diagrams of quaternary or more in consideration of all possible factors at once.

Even if main-phase single crystals have high magnetizations, high anisotropy fields, and high Curie temperatures, permanent magnets do not exhibit high performance without having appropriate microstructures, because microstructure interfaces play significant roles in preventing the magnetic domain-wall motion. While microstructure interfaces have been examined on the atomic scale obtaining insights into magnetic couplings between constituent

*Corresponding author
Email address: gohda.y.ab@m.titech.ac.jp (Yoshihiro Gohda)
[1] Present address: Institute for Solid State Physics, The University of Tokyo, Kashiwa 277-8581, Japan

phases [24–26], identification of phase equilibria requires quantification of the Gibbs free energy. Even though there have been successful attempts to evaluate the Gibbs free energy from first principles [27–36], such evaluations for general cases with sufficient precision can be computationally demanding due to, e.g., effects of the positional entropy due to displacements [37], and effects of anharmonic lattice vibrations such as the lift of the dynamical instability at finite temperatures. In contrast, the modeling of the Gibbs free energy to reproduce experimental phase equilibria, known as the CALPHAD (CALculation of PHAse Diagrams) approach [38], has been successful in providing thermodynamical database for multicomponent phase diagrams of, e.g., elements relevant to Nd-Fe-B permanent magnets [39]. Since Gibbs-energy functions are required for phases with experimentally unavailable compositions, the CALPHAD approach combined with first-principles calculations is effective [40–44]. Thus, such an approach should be promising also in the exploration of grain-boundary subphases of $SmFe_{12}$-based permanent magnets by examining phase equilibria through phase diagrams.

In this study, the ternary phase diagram for Sm-Fe-Cu is studied by the CALPHAD approach together with first-principles calculations. For compounds relevant to $SmFe_{12}$-based permanent magnets, CALPHAD Gibbs free energies are constructed with mixing enthalpies from first principles. Various phases including B2 Sm-Cu-Fe and $SmFe_{12}$ are examined using dilute alloys that is slightly off-stoichiometric. In addition, mixing enthalpies for the B2 phase are evaluated by the first-principles cluster-expansion method [45, 46], where the calculated Gibbs energy results in phase equilibria more consistent with experiments [15, 16]. We show that the liquid phase with compositions in the vicinity of Cu-45at.%Sm-1at.%Fe directly equilibrates with $SmFe_{12}$ above 1053 K opening up the possibility of the liquid-phase sintering. At lower temperatures, the equilibrating phase becomes nonmagnetic B2 Sm-Cu-Fe that is suitable as the grain-boundary phase. Since B2 Sm-Cu-Fe is much more stable than the amorphous phase, the grain-boundary phase may be crystalline depending on the cooling rate. Finite solubility of Fe into the B2 Sm-Cu phase comes from attractive interaction between Cu and Fe within the B2 sublattice, which is in contrast with repulsive one in binary Cu-Fe. The mechanism of the attractive interaction is the stabilization of Fe minority-spin states with lower single-electron energies compared with the case of binary SmFe.

2. Computational Details

We performed spin-polarized first-principles calculations to obtain total energies of the endmembers with the structures shown in Fig. 1 and their substituted solid solutions. The total energy of density functional theory (DFT) was self-consistently minimized using the frozen-core all-electron projector-augmented wave [47] (PAW) method as

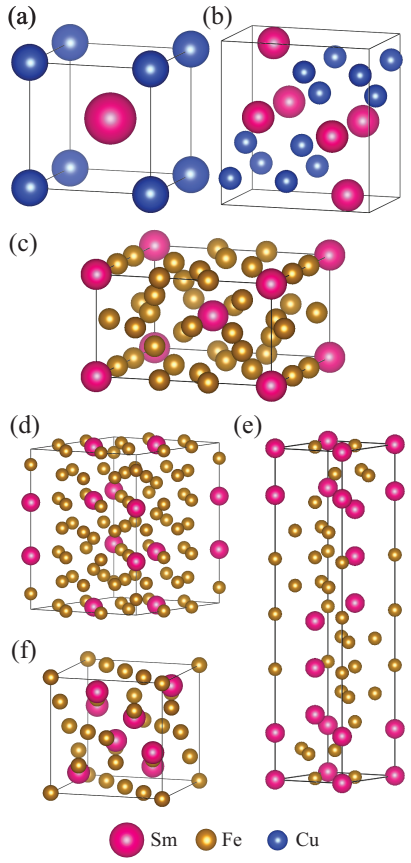

Figure 1: Atomic configurations of ordered binary Sm-Cu and Sm-Fe alloys: (a) B2 SmCu (CsCl type), (b) $SmCu_2$ ($CeCu_2$ type), (c) $SmFe_{12}$ ($ThMn_{12}$ type), (d) Sm_2Fe_{17} (Th_2Zn_{17} type), (e) $SmFe_3$ ($PuNi_3$ type), and (f) C15 $SmFe_2$ ($MgCu_2$ type).

implemented in the VASP code [48–50]. The exchange-correlation energy functional are treated using the generalized gradient approximation [51] parametrized as the form of Perdew–Burke–Ernzerhof [52]. ~~For Sm~~ It should be reasonable to assume that strongly localized $4f$ states hardly hybridize with other electronic states, even though some of Sm $4f$ states have single-electron energies close to the Fermi level [53]. Thus, an open-core PAW potential ~~were used~~ was used for Sm, where partially-occupied $4f$ electrons are kept frozen in the core. During the structure optimization, plane wave cutoff energy of 390 eV were used, and k-grid spacing were set as 0.1 $Å^{-1}$×0.1 $Å^{-1}$× 0.1 $Å^{-1}$. The full relaxed structures were obtained once atomic forces were smaller than 0.01 eV/Å with the total-energy convergence criterion of 10^{-7} eV. As initial spin configurations, Sm and Fe spins set as antiparallel, while spins within Sm and Fe were aligned as parallel.

Lattice models for mixing enthalpies H_{ij}^{mix} were constructed by the cluster-expansion method as implemented in the ATAT code [54, 55]. We considered binary mixing within one B2 sublattice for $X(Y_{1-y}Z_y)$ with the sublattice concentration y, where all possible 9 combinations of Sm, Cu, and Fe were examined for elements X, Y, and Z. In the cluster-expansion lattice model for the binary

mixing, $H_{ij}^{\rm mix}$ is described as

$$H_{ij}^{\rm mix} = \sum_{\alpha} J_{\alpha} \left\langle \prod_{I \in \alpha'} \sigma_I \right\rangle_{\alpha} \quad , \tag{1}$$

where α is the cluster type, J_α is the effective cluster interaction, and $\left\langle \prod_{I\in\alpha'} \sigma_I \right\rangle_\alpha$ is the correlation function of the cluster α. At each lattice point I, the variable σ_I in the binary model has the value of $+1$ or -1 depending on elements. We considered up to tetrahedron clusters. The effective cluster interaction was determined by fittings to reproduce the mixing enthalpy obtained by first-principles calculations. In order to consider only structures that can be recognized as B2, structures with lattice vectors deviating from those of the ideal B2 lattice significantly were excluded from the fitting with the criterion R of more than 9%, where R is defined as

$$R = \sqrt{\sum_{i,j} \varepsilon_{ij}^2} \quad , \tag{2}$$

where $\{\varepsilon_{ij}\}$ are the eigenstrains induced by the relaxation from the B2 structure, i.e., other than the isotropic scaling and the rigid rotation [56]. In addition, structures with large distortions by atomic displacements were excluded so that the cross-validation score for the fitting of J_α becomes smaller than 65 meV per atom.

In the CALPHAD approach, the sub-regular solution model is used to describe Gibbs energies of phases that are considered in phase diagrams of interest. In the sub-regular solution model, the Gibbs energy is decomposed into three terms: (i) linear combination of Gibbs energies of endmembers, (ii) the configurational-entropy term within the Bragg-Williams approximation, and (iii) the excess Gibbs energy as all effects other than the former two terms. We used the two-sublattice model for intermetallic compounds, where the Gibbs energy of a binary stoichiometric compound, e.g., the B2 phase is described as an endmember by the two-sublattice model. The Gibbs energy of endmembers with the magnetization at low temperatures was described by adding a magnetic term based on the Inden model [57, 58]. In this study, we constructed Gibbs-energy functions of $SmFe_{12}$ as well as experimentally unavailable counterparts of Sm-Fe and Sm-Cu compounds, while preexisting Gibbs-energy databases were used for all other endmembers [59–62]. The Kopp-Neumann rule for the specific heat indicates that the temperature dependence of excess Gibbs energies can be linear. Assuming this linear dependence is small in the present study, mixing enthalpies obtained from first principles were used for phases shown in Fig. 1 as excess Gibbs energies in the present study, details of which are given in the following. Using Gibbs energies as inputs, phase diagrams were calculated by the PANDAT code [63].

3. Results and Discussion

3.1. Mixing enthalpy

Figure 2 shows mixing enthalpies $H_{ij}^{\rm mix}$ between B2 Sm-Cu-Fe stoichiometric compounds as endmembers in the two-sublattice model. Even though the ground-state structure of SmCu is the B27 (FeB-b) structure [24], we focus on the B2 structure in the present study, because high-temperature phases are of our primary interest. From Figs. 2(a) and (b), it is clear that the interaction between Sm and Cu is repulsive within each sublattice of B2 SmCu. This means that each sublattice of binary B2 SmCu does not allow the alloying of Sm-Cu at zero temperature. In addition, substitutional Fe impurities in B2 SmCu are more stable at Cu sites than at Sm sites as seen in Figs. 2 (g) and (i). Other mixing enthalpies are also used to construct the Gibbs-energy landscape in the whole Sm-Fe-Cu compositions.

The mixing enthalpy is of importance to evaluate the Gibbs energy beyond the ideal-solution model through the Redlich-Kister polynomial $L_{k:i,j}$. In the present CALPHAD two-sublattice model, $H_{ij}^{\rm mix}$ and $L_{k:i,j}$ has the relation, $H_{ij}^{\rm mix} = y_j(1-y_j)L_{k:i,j}$, where y_i the sublattice concentration of the element i. Since the mixing enthalpy depends on specific atomic configuration, we adopted the case of the disorder limit. Curves for this disorder limit shown in Fig. 2 are obtained from the cluster-expansion model as

$$\begin{aligned} H_{ij}^{\rm mix}(y_j) &= \sum_{\alpha} J_{\alpha} \prod_{I\in\alpha'} \langle \sigma_I \rangle_{\alpha} \\ &= \sum_{\alpha} J_{\alpha} (2y_j - 1)^{k_\alpha} \quad , \end{aligned} \tag{3}$$

where k_α is the order of a cluster, e.g., $k_\alpha = 3$ for triangle clusters. Figure 2 also includes results obtained by fitting from the dilute alloys that are slightly off-stoichiometric from the endmembers. In some cases, the cluster-expansion model significantly improves the mixing enthalpy compared with the dilute-alloy approach. Thus, mixing enthalpy from the cluster-expansion model is used for the B2 phase unless otherwise stated, while the dilute alloys are used to evaluate mixing enthalpies of the rest of the phases shown in Fig. 1 that are found to be of less importance considering roughly-estimated phase equilibria. These mixing enthalpies are added to CALPHAD Gibbs energies as an approximation of the excess Gibbs energy. Other phases including the liquid phase are considered using existing Gibbs-energy functions [60–62] to examine phase equilibria reported below.

In the evaluation of the mixing enthalpy from first principles, it was assumed that one of the sublattice is always occupied by one element. On the other hand, this assumption is lifted in examining phase equilibria by using the condition

$$\frac{\partial G}{\partial y_i^{(n)}} = 0 \quad , \tag{4}$$

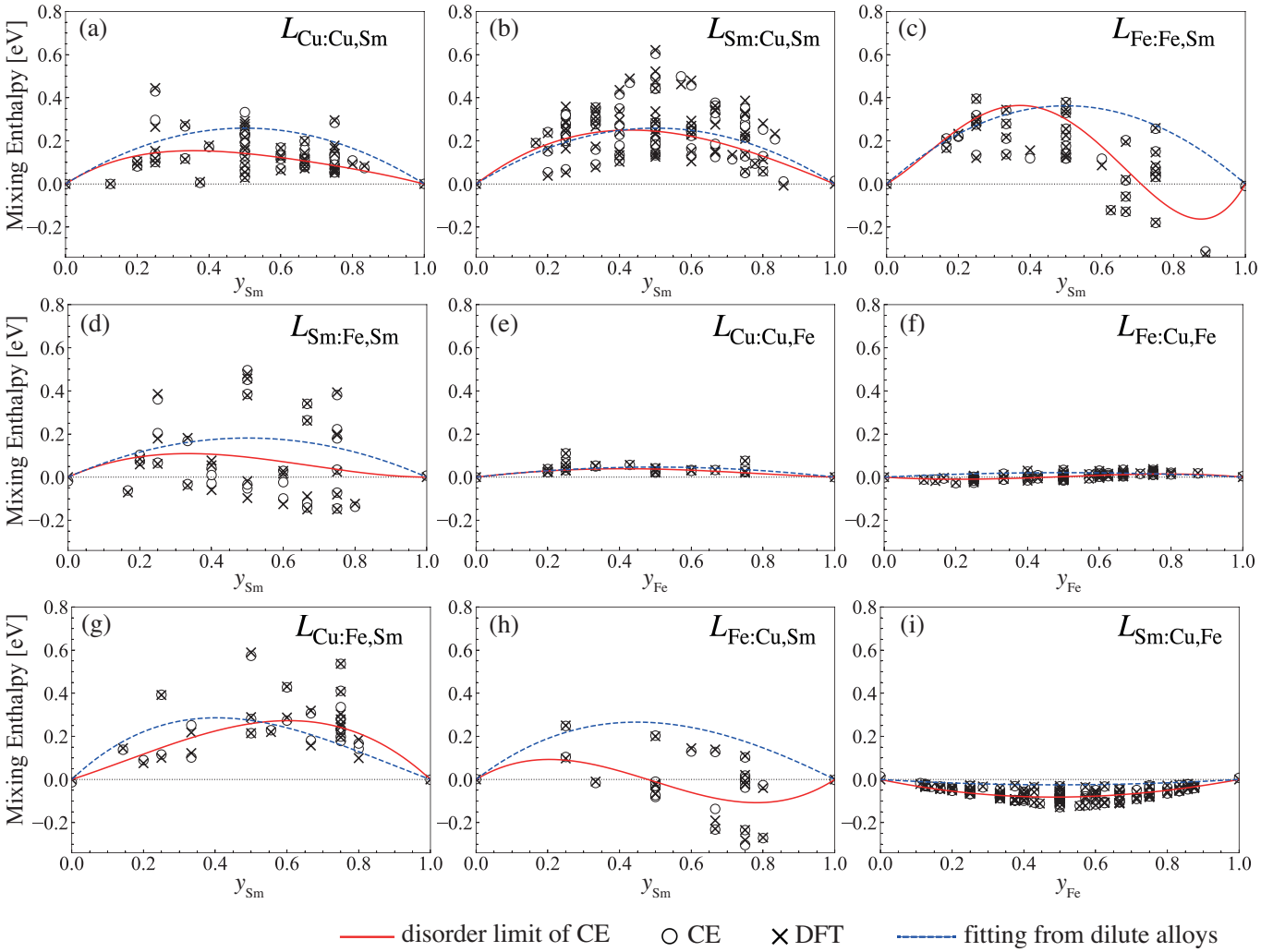

Figure 2: The mixing enthalpy $H_{ij}^{\rm mix}$ between B2 stoichiometric compounds that is related to the Redlich-Kister polynomial $L_{k:i,j}$ in the present CALPHAD two-sublattice model through $H_{ij}^{\rm mix} = y_j(1-y_j)L_{k:i,j}$: (a) $H_{\rm CuSm}^{\rm mix}$ of $({\rm Sm}_{y_{\rm Sm}}{\rm Cu}_{1-y_{\rm Sm}}){\rm Cu}$, (b) $H_{\rm CuSm}^{\rm mix}$ of ${\rm Sm}({\rm Cu}_{1-y_{\rm Sm}}{\rm Sm}_{y_{\rm Sm}})$, (c) $H_{\rm FeSm}^{\rm mix}$ of $({\rm Sm}_{y_{\rm Sm}}{\rm Fe}_{1-y_{\rm Sm}}){\rm Fe}$, (d) $H_{\rm FeSm}^{\rm mix}$ of ${\rm Sm}({\rm Fe}_{1-y_{\rm Sm}}{\rm Sm}_{y_{\rm Sm}})$, (e) $H_{\rm CuFe}^{\rm mix}$ of $({\rm Fe}_{y_{\rm Fe}}{\rm Cu}_{1-y_{\rm Fe}}){\rm Cu}$, (f) $H_{\rm CuFe}^{\rm mix}$ of ${\rm Fe}({\rm Cu}_{1-y_{\rm Fe}}{\rm Fe}_{y_{\rm Fe}})$, (g) $H_{\rm FeSm}^{\rm mix}$ of $({\rm Sm}_{y_{\rm Sm}}{\rm Fe}_{1-y_{\rm Sm}}){\rm Cu}$, (h) $H_{\rm CuSm}^{\rm mix}$ of $({\rm Sm}_{y_{\rm Sm}}{\rm Cu}_{1-y_{\rm Sm}}){\rm Fe}$, (i) $H_{\rm CuFe}^{\rm mix}$ of ${\rm Sm}({\rm Cu}_{1-y_{\rm Fe}}{\rm Fe}_{y_{\rm Fe}})$. Note that the first and second sublattices are equivalent, i.e., $L_{k:i,j} = L_{i,j:k}$. Values directly obtained by first-principles DFT calculations are represented by crosses. Circles are $H_{ij}^{\rm mix}$ from cluster-expansion (CE) model for configurations same as crosses. Red solid lines indicate the disorder limit of the CE model that are used in the CALPHAD model through $L_{k:i,j}$. Blue dashed lines are fitted curves from results of first-principles calculations for dilute alloys that are slightly off-stoichiometric from the endmembers.

where $y_i^{(n)}$ is the sublattice concentration of the element i in the sublattice n. With the above constraint, the elements can occupy on both sublattices of the B2 structure as $({\rm Sm,Cu,Fe})_1({\rm Cu,Fe,Sm})_1$ ~~.~~ in the two-sublattice model. In this study, the Gibbs-energy function per atom of the B2 phase within the two-sublattice model is given as

$$G_{\rm B2} = \sum_{ij} y_i^{(1)} y_j^{(2)} G_{ij} + \frac{1}{2} k_{\rm B} T \sum_{n=1}^{2} \sum_{i} y_i^{(n)} \log y_i^{(n)} + \sum_{ik} \sum_{j>i} \left[y_k^{(1)} y_i^{(2)} y_j^{(2)} L_{k:i,j} + y_k^{(2)} y_i^{(1)} y_j^{(1)} L_{i,j:k} \right] \quad (5)$$

where $\{G_{ij}\} = \{G_{\rm bcc-Fe}, G_{\rm bcc-Sm}, G_{\rm bcc-Cu}, G_{\rm B2-SmCu}, G_{\rm B2-SmFe}, G_{\rm B2-FeCu}, \}$, $k_{\rm B}$ is the Boltzmann constant, T is the temperature, and

$$L_{k:i,j} = \sum_{\kappa=0}^{2} L_{k:i,j}^{(\kappa)} \left(y_i^{(2)} - y_j^{(2)} \right)^{\kappa} \quad . \quad (6)$$

Parameters $\{L_{k:i,j}^{(\kappa)}\}$ are obtained from $\{J_\alpha\}$. Numerical values of parameters appearing in the above formulae are provided in the unit of J ~~/mol~~ per mole of atoms as Supplemental Material. ~~Other phases including the liquid phase are considered using existing Gibbs-energy functions [60–62] to examine phase equilibria reported below.~~

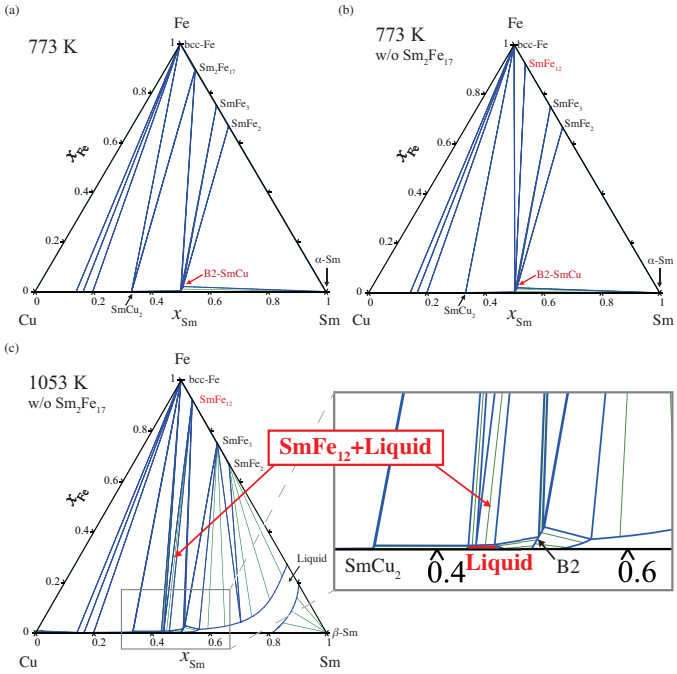

Figure 3: (a) Ternary phase diagram of the Sm-Fe-Cu system at 773 K. (b) Phase diagram excluding the Sm_2Fe_{17} phase from (a) assuming the stabilization of the $SmFe_{12}$ phase due to possible additive elements. (c) Ternary phase diagram of the the Sm-Fe-Cu system excluding the Sm_2Fe_{17} phase at 1053 K. In all cases, the CALPHAD Gibbs energy obtained with Redlich-Kister polynomials $L_{k:i,j}$ from the cluster-expansion method is used for the B2 phase.

3.2. Phase equilibria

The Cu-Fe, Sm-Cu, and Sm-Fe binary system have been critically assessed by Turchanin et al. [60], Zhuang et al. [61], and Chen et al. [62], respectively. We adopted these assessments for the Sm-Fe-Cu ternary system. Since $SmFe_{12}$ in the Sm-Fe binary system is metastable, and, thus, the formation energy of $SmFe_{12}$ was estimated from first principles. As a finite-temperature effect, the formation entropy was given so as $SmFe_{12}$ became stable when Sm_2Fe_{17} was excluded from the equilibrium calculations. The magnetic excess Gibbs energy was given by Inden model [57, 58] with the following two parameters: the Curie temperature of the compound was set as 555 K measured approximately in experiments [4], and the thermodynamic effective magnetic moment was set as 1 μ_B [4], where μ_B is the Bohr magneton. The obtained Gibbs energy of the $SmFe_{12}$ as an endmember is given in Appendix.

For the calculations of the phase equilibria in the ternary system, solubility of the third element to the binary compounds were considered by the cluster-expansion formalism for the B2 phase, while dilute-alloy models were used for other structures shown in Fig. 1. Even though the cluster-expansion formalism obviously provides more reliable results, changes by the use of dilute-alloy models for other phases are expected to be minor in phase equilibria, due to their limited solubility (approximately 1 at.%) in the phases evaluated by dilute-alloy models. The Gibbs energy of the phases considered are written in the TDB format, which is accepted for various thermodynamic software packages such as PANDAT [63] and Thermo-Calc [64]. The TDB file is provided as Supplemental Material.

The isothermal section at 773 K is presented as a function of the compositions $\{x_i\}$ in Fig. 3(a). The calculated phase diagram agrees well with the experimentally reported one [15]. In the present calculations, the preferential site of Fe in the B2 structure is the Cu site as expected from the mixing enthalpy mentioned above, which is in good agreement with the experiments [15]. The solubility of Fe in the B2 SmCu is estimated to be 2 at.% that qualitatively agrees with 5.8 at.% reported experimentally with the annealing at 723 K for relatively short time of 48 h [15]. It has recently been found using first-principles thermodynamics that the theoretical Fe solubility should increase by taking the Gibbs energy of the B27 phase into account [65].

Even though the stability of Sm_2Fe_{17} overwhelms that of $SmFe_{12}$ in the Sm-Fe-Cu ternary system, the relative stability can be modulated by doping of other elements into $SmFe_{12}$. Assuming such stabilization of pseudobinary $SmFe_{12}$ compared with Sm_2Fe_{17}, we exclude the Gibbs energy of Sm_2Fe_{17} from the phase diagram. As presented in Fig. 3(b), $SmFe_{12}$ becomes stable appearing in the phase diagram instead of Sm_2Fe_{17}. At elevated temperatures, $SmFe_{12}$ can be directly in equilibrium with the liquid phase in alloy compositions around Cu-45at.%Sm-1at.%Fe, as far as the precipitation of Sm_2Fe_{17} is suppressed. The isothermal section at 1053 K is shown in Fig. 3(c), where the liquid-$SmFe_{12}$ two-phase regions are indicated with red arrows. This two-phase equilibrium suggests that the liquid-phase sintering of the $SmFe_{12}$-based magnets should be possible without inducing the precipitation of bcc Fe. For the liquid phase with Cu compositions of at least 50 at.%, the two-phase equilibrium appears in a temperature range of 1049–1163 K. In addition, the grain-boundary subphase appearing with the solidification of this liquid phase is expected to have compositions similar to that of the liquid phase. Thus, the subphase becomes nonmagnetic as confirmed by first-principles calculations. The nonmagnetic behavior of the subphase is preferable because it hinders magnetic domain walls from propagating. In experiments, $Sm_{12}Fe_{74}V_{12}Cu_2$ alloys have high concentrations of Sm and Cu at intergranular regions, even though the alloy composition may be too Sm rich [17]. The theoretical findings in this study can be compared with these experimental observations and should be utilized to design the microstructures in more details.

The $Sm_{0.5}Cu_{0.5}$-$Sm_{0.5}Fe_{0.5}$ transverse sections of the ternary system are presented in Fig. 4 to compare effects of the excess Gibbs energies estimated from the cluster-expansion method and from the dilute alloys. For the case where the Gibbs energy of mixing is estimated from the dilute alloys, Fe has a negligibly limited solubility to the B2 structure as seen in Fig. 4 (b), whereas the Gibbs energy of mixing estimated from the cluster-expansion method

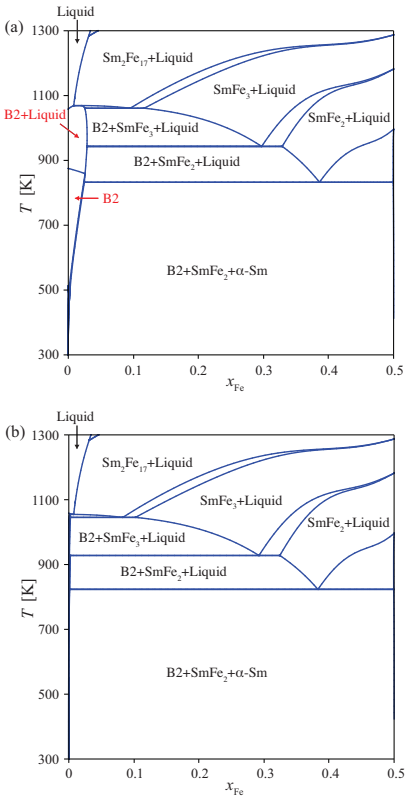

Figure 4: Pseudobinary phase diagram of $Sm_{0.5}Cu_{0.5-x_{Fe}}Fe_{x_{Fe}}$. The Gibbs energy of the B2 phase, i.e., $Sm(Cu_{1-y_{Fe}}Fe_{y_{Fe}})$, is obtained with Redlich-Kister polynomials $L_{k:i,j}$ (a) from the cluster-expansion method and (b) from dilute alloys.

results in a much wider area of the B2 single phase as indicated with the red arrows in Fig. 4(a). The use of the cluster-expansion method improves the description of the B2 phase substantially, because this wider solubility of Fe is consistent with experimental result [15] as was already mentioned. The discrepancy in the dilute-alloy approach comes from significant underestimation of the magnitude of the mixing enthalpy as shown in Fig. 2(i).

3.3. Interaction between Cu and Fe

It is well established that Cu and Fe are repulsive with each other in the Cu-Fe binary system. This fact is seen in the Cu-Fe binary phase diagram as the phase separation. The repulsive interaction makes the mixing enthalpy positive that can be seen for the A2 and B2 phases in Fig. 5(a). The result for the $Sm(Cu_{1-y_{Fe}}Fe_{y_{Fe}})$ B2 phase makes remarkable contrast with the Cu-Fe binary case as seen in Fig. 2(i), where the interaction between Cu and Fe becomes attractive within the B2 sublattices of $Sm(Cu_{1-y_{Fe}}Fe_{y_{Fe}})$. This attractive interaction is the origin of the Fe solubility into the B2 phase that is clear from the pseudobinary phase diagram in Fig. 4(a).

Differences in the attractive interaction in ternary Sm-Cu-Fe and the repulsive one in binary Cu-Fe can be understood by the local density of states (LDOS) shown in Figs. 5(b), (c), and (d). Here, we chose ordered B2 and

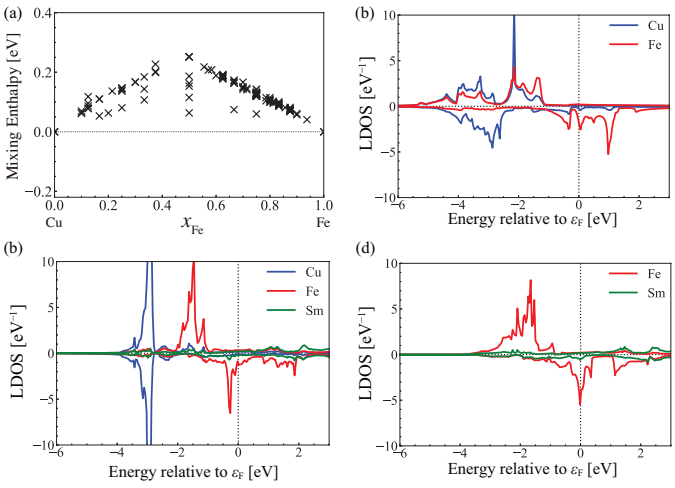

Figure 5: (a) Mixing enthalpy of $Cu_{1-x_{Fe}}Fe_{x_{Fe}}$ in the A2 bcc phase and the B2 phase obtained by first-principles calculations. Atom-projected local density of states (LDOS) for (b) B2 CuFe, (c) $L2_1$ Sm_2CuFe, and (d) B2 SmFe.

$L2_1$ structures as representative atomic configurations for convenience. It is clear from Fig. 5(b) that $3d$ states of Cu and Fe strongly hybridize with each other in binary Cu-Fe creating broad $3d$ bands. Energies of minority-spin Cu $3d$ states become in average higher by the hybridization compared with the case of the Cu single phase, which makes the Cu-Fe interaction repulsive. In addition, minority-spin Fe $3d$ states have a high peak at the Fermi level ε_F also contributing to repulsive interaction. Note that the LDOS of the majority spin at ε_F is nonzero due to $4s$ bands with wide dispersions. In contrast, overlaps between $3d$ bands of Cu and Fe are considerably small in ternary Sm-Cu-Fe as is seen in Fig. 5(c), hence repulsive interaction between Cu and Fe is absent. Compared with the phase-separated case of SmFe and SmCu, Fe in Sm-Cu-Fe is stabilized by an avoided peak of the minority-spin Fe LDOS at ~~the Fermi level~~ ε_F that differs significantly from the case of SmFe in Fig. 5(d). The attractive interaction between Cu and Fe within the B2 phase makes the B2 phase more stable than the amorphous phase. This result indicates that the grain-boundary subphase in $SmFe_{12}$-based sintered magnets can be crystalline depending on the cooling rate in the sintering process. The stability of the crystalline B2 phase even in equilibrium can be considered as a potential advantage, because a crystalline grain-boundary subphase might contribute to alignment of the main-phase grains improving the coercivity significantly.

In addition to $L2_1$, we examine the stability of the so-called XA structure that is a variant structure of Heusler alloys relevant to spintronics [66–68]. The XA Sm_2CuFe was found to be unstable against phase separations: H^{mix} relative to B2 SmCu and B2 SmFe is 172 meV/atom, whereas H^{mix} relative to bcc Sm and B2 CuFe is 85 meV/atom. The values for $L2_1$ Sm_2CuFe are −69 meV/atom and −155 meV/atom, respectively.

4. Conclusion

We applied first-principles calculations to the CALPHAD method and calculated the Sm-Fe-Cu ternary phase diagram. Formation energies of metastable stoichiometric endmembers including $SmFe_{12}$ were calculated by DFT to construct Gibbs energies within the so-called compound energy formalism. Mixing enthalpies of dilute alloys were also calculated to determine the interaction parameters of substituted solid solutions. Moreover, the Gibbs energy for the B2 phase, which is a candidate for the grain-boundary subphase of $SmFe_{12}$-based magnets, was evaluated by the first-principles cluster-expansion method to improve the accuracy. Mixing enthalpies among B2 endmembers were converted to the Redlich-Kister polynomial that represents the effect of second-nearest-neighbor interactions in the B2 structure. The thermodynamic database of this study reproduces the finite solid solution of Fe in B2 SmCu in agreement with experiments. We have found that this solubility is attributed to the attractive interaction between Fe and Cu in B2 Sm(Cu,Fe) solid solutions, which is in contrast with the repulsive one in binary Cu-Fe. Furthermore, phase equilibria of the $SmFe_{12}$ phase and the Sm-Cu-Fe alloys were investigated. We identified that the liquid phase with compositions about Cu-45at.% Sm-1at.%Fe directly equilibrates with $SmFe_{12}$ above 1053 K. At lower temperatures, the equilibrating phase becomes B2 Sm-Cu-Fe. Since B2 Sm-Cu-Fe is much more stable than the amorphous phase, the grain-boundary phase may be crystalline depending on the cooling rate. In the development of $SmFe_{12}$-based magnets, these phases are expected to suppress the precipitation of bcc Fe associated with thermal decomposition of 1-12 grain surfaces as well as the magnetic interaction between 1-12 grains.

Acknowledgements

The authors thank Dr. Arkapol Saengdeejing for fruitful discussions. This work was partly supported by MEXT as Fugaku-DPMSD (Grant No. JPMXP1020200307) and as DXMag (Grant No. JPMXP1122715503). The calculations were partly carried out by using supercomputers at ISSP, The University of Tokyo, and TSUBAME, Tokyo Institute of Technology, as well as the supercomputer Fugaku, RIKEN (Project No. hp220175).

Appendix A. Gibbs-energy function of $SmFe_{12}$

For the stoichiometric $SmFe_{12}$ intermetallic compound as an endmember, the assessed Gibbs-energy function is given in the unit of J/mol as:

$$G_{SmFe_{12}} = a + bT + \frac{12}{13}G_{bcc-Fe} + \frac{1}{12}G_{\alpha-Sm} + G^{mag} \quad , \tag{A.1}$$

where $a = -6270$ J/mol, $b = 4$ J/molK, G_{bcc-Fe} and $G_{\alpha-Sm}$ are the Gibbs energies of pure bcc Fe and pure α Sm, respectively [59], and G^{mag} is the magnetic excess Gibbs energy [57, 58] with the parameters given in the main text. Full list of Gibbs energies used to examine phase equilibria in this study is summarized in Supplemental Material as a TDB file. The file extension should be changed from .txt to .tdb for the use of thermodynamic software.

References

[1] K. Ohashi, Y. Tawara, R. Osugi, and M. Shimao, Magnetic properties of Fe-rich rare-earth intermetallic compounds with a $ThMn_{12}$ structure, J. Appl. Phys. **64** (1988) 5714-5716.

[2] D. Wang, S. H. Liou, P. He, D. J. Sellmyer, G. C. Hadjipanayis, and Y. Zhang, $SmFe_{12}$ and $SmFe_{12}N_x$ films fabricated by sputtering, J. Magn. Magn. Mater. **124** (1993) 62-68.

[3] T. Saito, H. Miyoshi, and D. Nishio-Hamane, Magnetic properties of Sm-Fe-Ti nanocomposite magnets with a $ThMn_{12}$ structure, J. Alloys Compd. **519** (2012) 144-148.

[4] Y. Hirayama, Y. K. Takahashi, S. Hirosawa, and K. Hono, Intrinsic hard magnetic properties of $Sm(Fe_{1-x}Co_x)_{12}$ compound with the $ThMn_{12}$ structure, Scr. Mater. **138** (2017) 62-65.

[5] H. S. Li and J. M. D. Coey, Magnetic properties of ternary rare-earth transition-metal compounds, in Handb. Magn. Mater., vol. 6, 1-83 (Elsevier, North Holland, 1991).

[6] T. Kuno, S. Suzuki, K. Urushibata, K. Kobayashi, N. Sakuma, M. Yano, A. Kato, and A. Manabe, $(Sm,Zr)(Fe,Co)_{11.0-11.5}Ti_{1.0-0.5}$ compounds as new permanent magnet materials, AIP Adv. **6** (2016) 025221.

[7] K. Kobayashi, S. Suzuki, T. Kuno, K. Urushihara, N. Sakuma, M. Yano, T. Shouji, A. Kato, and A. Manabe, The stability of newly developed $(R,Zr)(Fe,Co)_{12-x}Ti_x$ alloys for permanent magnets, J. Alloys Compd. **694** (2017) 914-920.

[8] P. Tozman, H. Sepehri-Amin, Y. K. Takahashi, S. Hirosawa, and K. Hono, Intrinsic magnetic properties of $Sm(Fe_{1-x}Co_x)_{11}Ti$ and Zr-substituted $Sm_{1-y}Zr_y(Fe_{0.8}Co_{0.2})_{11.5}Ti_{0.5}$ compounds with $ThMn_{12}$ structure toward the development of permanent magnets, Acta Mater. **153** (2018) 354-363.

[9] P. Tozman, T. Fukazawa, D. Ogawa, H. Sepehri-Amin, A. Bolyachkin, T. Miyake, S. Hirosawa, K. Hono, and Y.K. Takahashi, Peculiar behavior of V on the Curie temperature and anisotropy field of $SmFe_{12-x}V_x$ compounds, Acta Mater. **232** (2022) 117928.

[10] I. Dirba, Y. Harashima, H. Sepehri-Amin, T. Ohkubo, T. Miyake, S. Hirosawa, and K.Hono, Thermal decomposition of $ThMn_{12}$-type phase and its optimum stabilizing elements in $SmFe_{12}$-based alloys, J. Alloys Compd. **813** (2020) 152224.

[11] L. Zhao, R. Su, L. Wen, W. Li, X. L. Liu, Z. H. Zhang, R. Z. Zhao, Y. Y. Han, and X. F. Zhang, Intrinsically High Magnetic Performance in Core-Shell Structural $(Sm,Y)Fe_{12}$-Based Permanent Magnets, Adv. Mater. **34** (2022) 2203503.

[12] H. Sepehri-Amin, Y. Tamazawa, M. Kambayashi, G. Saito, Y. K. Takahashi, D. Ogawa, T. Ohkubo, S. Hirosawa, M. Doi, T. Shima, and K. Hono, Achievement of high coercivity in $Sm(Fe_{0.8}Co_{0.2})_{12}$ anisotropic magnetic thin film by boron doping, Acta Mater. **194** (2020) 337-342.

[13] T. Fukazawa, H. Akai, Y. Harashima, and T.Miyake, First-principles study of intersite magnetic couplings and curie temperature in $RFe_{12-x}Cr_x$ (R = Y, Nd, Sm), J. Phys. Soc. Jpn. **87** (2018) 044706.

[14] Y. Harashima, T. Fukazawa, H. Kino, and T. Miyake, Effect of R-site substitution and the pressure on stability of RFe_{12}: A first-principles study, J. Appl. Phys. **124** (2018) 163902.

[15] C. Lu, X. Hong, X. Bao, X. Gao, and J. Zhu, Changing phase equilibria: A method for microstructure optimization and properties improvement in preparing anisotropic $Sm_2Fe_{17}N_3$ powders, J. Alloys Compd. **784** (2019) 980-989.

[16] O. Takeda, K. Shimizu, H. Zhu, and S. Sugimoto, Phase equilibria of Sm-Fe-Ti-M (M=Cu, Ag) systems and wetting behavior

of M–Sm alloys on $SmFe_{11}Ti$ substrate, J. Magn. Magn. Mater. **542** (2022) 168620.
[17] A.M. Schönhöbel, R. Madugundo, J.M. Barandiarán, G.C. Hadjipanayis, D. Palanisamy, T. Schwarz, B. Gault, D. Raabe, K. Skokov, O. Gutfleisch, J. Fischbacher, and T. Schrefl, Nanocrystalline Sm-based 1:12 magnets, Acta Mater. **200** (2020) 652-658.
[18] A.M. Schönhöbel, R. Madugundo, A.M. Gabay, and J.M. Barandiaŕan, The Sm-Fe-V based 1:12 bulk magnets, J. Alloys Compd. **791** (2019) 1122-112.
[19] A.M. Gabay, C. Han, C. Ni, and G.C. Hadjipanayis, Effect of alloying with Sc, Nb and Zr on reduction-diffusion synthesis of magnetically hard $Sm(Fe,Co,Ti)_{12}$-based monocrystalline powders, J. Magn. Magn. Mater. **541** (2022) 168550.
[20] A.M.Gabay and G.C. Hadjipanayis, Microstructure and Hard Magnetic Properties of $Sm_{1-x}Zr_x(Fe,Co)_{11.3-y}Ti_{0.7}B_y$ Ingots and Thick Melt-Spun Ribbons, IEEE Trans. Magn. **58** (2022) 2100805.
[21] A.M.Gabay and G.C. Hadjipanayis, Isotropic nanocrystalline $Sm(Fe,Co)_{11.3}Ti_{0.7}$ magnets modified with B and Zr, J. Magn. Magn. Mater. **529** (2021) 167867.
[22] A.M. Gabay, C. Han, C. Ni, and G.C. Hadjipanayis, Re-investigation of high-temperature phase equilibria in Fe-rich Sm–Fe–Ti alloys, J. Alloys Compd. **947** (2023) 169520.
[23] A.M. Gabay and G.C. Hadjipanayis, High-coercivity $ThMn_{12}$-type monocrystalline Sm–Zr–Fe–Co–Ti particles by high-temperature reduction diffusion, Scr. Mater. **196** (2021) 113760.
[24] Y. Ainai, T. Shiozawa, Y. Tatetsu, and Y. Gohda, First-principles study on surface stability and interface magnetic properties of $SmFe_{12}$, Appl. Phys. Express **13** (2020) 045502.
[25] Y. Gohda, First-principles determination of intergranular atomic arrangements and magnetic properties in rare-earth permanent magnets, Sci. Technol. Adv. Mater. **22** (2021) 113-123.
[26] Y. Gohda, Y. Tatetsu, and S. Tsuneyuki, Electron Theory on Grain-Boundary Structures and Local Magnetic Properties of Neodymium Magnets, Mater. Trans. **59** (2018) 332-337.
[27] T. Mohri, S. Takizawa, and K. Terakura, First-principles calculation of heats of formation for Au-Cu, Au-Pd and Au-Ag alloys with thermal vibration effects, J. Phys.: Condens. Matter **5** (1993) 1473-1480.
[28] P. Pavone, S. Baroni, and S. de Gironcoli, $\alpha \leftrightarrow \beta$ phase transition in tin: A theoretical study based on density-functional perturbation theory, Phys. Rev. B **57** (1998) 10421-10423.
[29] J.-C. Crivello and J.-M. Joubert, First principles calculations of the σ and χ phases in the Mo-Re and W-Re systems, J. Phys.: Condens. Matter **22** (2010) 035402.
[30] F. Körmann, A. Dick, T. Hickel, and J. Neugebauer, Role of spin quantization in determining the thermodynamic properties of magnetic transition metals, Phys. Rev. B **83** (2011) 165114.
[31] A. van de Walle, Methods for First-Principles Alloy Thermodynamics, JOM **65** (2013) 1523–1532.
[32] M. Palumbo, S. G. Fries, A. Dal Corso, F. Körmann, T. Hickel, and J. Neugebauer, Reliability evaluation of thermophysical properties from first-principles calculations, J. Phys.: Condens. Matter **26** (2014) 335401.
[33] T. Mohri, Cluster Variation Method as a Theoretical Tool for the Study of Phase Transformation, Metall. Mater. Trans. A **48** (2017) 2753-2770.
[34] T. Tanaka and Y. Gohda, Prediction of the Curie temperature considering the dependence of the phonon free energy on magnetic states, npj Comput. Mater. **6** (2020) 184.
[35] T. Tanaka and Y. Gohda, First-Principles Study of Magnetism-Dependent Phonons Governed by Exchange Ligand Field, J. Phys. Soc. Jpn. **89** (2020) 093705.
[36] A. Saengdeejing and Y. Chen, Improving Thermodynamic Stability of $SmFe_{12}$-Type Permanent Magnets from High Entropy Effect, J. Phase Equilib. Diffus. **42** (2021) 592-605.
[37] R. Yamada, M. Ohno, and T. Mohri, Configurational kinetics studied by Path Probability Method, Prog. Mater. Sci. **120** (2021) 100765.
[38] N. Saunders and A. P. Miodownik, CALPHAD : calculation of phase diagrams : a comprehensive guide, (Elsevier, North Holland, 1998).
[39] T. Abe, M. Morishita, Y. Chen, A. Saengdeejing, K. Hashimoto, Y. Kobayashi, I. Ohnuma, T. Koyama, and S. Hirosawa, Development of a prototype thermodynamic database for Nd-Fe-B permanent magnets, Sci. Technol. Adv. Mater. **22** (2021) 557-570.
[40] P. E. A. Turchi, V. Drchal, J. Kudrnovsky, C. Colinet, L. Kaufman, and Z. K. Liu, Application of ab initio and CALPHAD thermodynamics to Mo-Ta-W alloys, Phys. Rev. B **71** (2005) 094206.
[41] A. Berche, J. C. Tédenac, and P. Jund, Ab-initio calculations and CALPHAD description of Cr-Ge-Mn and Cr-Ge-Si, Calphad **49** (2015) 50-57.
[42] A. Saengdeejing, Y. Chen, M. Matsuura, S. Sugimoto, First-principles study of stability of Cu in the Nd-rich and Nd oxide phases of Nd-Fe-B permanent magnet, J. Chin. Chem. Soc. **63** (2016) 506-512.
[43] A. Saengdeejing, Y. Chen, O. Takeda, M. Enoki, S. Sugimoto, H. Ohtani, and T. Abe, Sm-Ti binary thermodynamic database and phase diagram, Calphad **75** (2021) 102357.
[44] W. Xiong, Q. Chen, P. A. Korzhavyi, and M. Selleby, An improved magnetic model for thermodynamic modeling, Calphad **39** (2012) 11-20.
[45] J. W. D. Connolly and A. R. Williams, Density-functional theory applied to phase transformations in transition-metal alloys, Phys. Rev. B **27** (1983) 5169-5172.
[46] J. M. Sanchez, F. Ducastelle, and D. Gratias, Generalized cluster description of multicomponent systems, Physica A **128** (1984) 334-350.
[47] P. E. Blöchl, Projector augmented-wave method, Phys. Rev. B **50** (1994) 17953-17979.
[48] G. Kresse and J. Hafner, *Ab initio* molecular dynamics for open-shell transition metals Phys. Rev. B **48** (1993) 13115-13118.
[49] G. Kresse and J. Furthmüller, Efficient iterative schemes for *ab initio* total-energy calculations using a plane-wave basis set, Phys. Rev. B **54**, (1996) 11169-11186.
[50] G. Kresse and D. Joubert, From ultrasoft pseudopotentials to the projector augmented-wave method, Phys. Rev. B **59** (1999) 1758-1775.
[51] J. P. Perdew, J. A. Chevary, S. H. Vosko, K. A. Jackson, M. R. Pederson, D. J. Singh, and C. Fiolhais, Atoms, molecules, solids, and surfaces: Applications of the generalized gradient approximation for exchange and correlation, Phys. Rev. B **46** (1992) 6671-6687.
[52] J. P. Perdew, K. Burke, and M. Ernzerhof, Generalized Gradient Approximation Made Simple, Phys. Rev. Lett. **77** (1996) 3865-3868.
[53] X.B. Liu and Z. Altounian, Magnetic moments and exchange interaction in $Sm(Co,Fe)_5$ from first-principles, Comput. Mater. Sci. **50** (2011) 841-846.
[54] A. van de Walle, M. Asta, and G. Ceder, The alloy theoretic automated toolkit: A user guide, Calphad **26** (2002) 539-553.
[55] A. van de Walle and M. Asta, Self-driven lattice-model Monte Carlo simulations of alloy thermodynamic properties and phase diagrams, Modell. Simul. Mater. Sci. Eng. **10** (2002) 521-538.
[56] G. Ghosh, A. van de Walle, and M. Asta, First-principles calculations of the structural and thermodynamic properties of bcc, fcc and hcp solid solutions in the Al-TM (TM=Ti, Zr and Hf) systems: A comparison of cluster expansion and supercell methods Acta Mater. **56** (2008) 3202-3221.
[57] G. Inden, The role of magnetism in the calculation of phase diagrams, Physica B+C **103** (1981) 82-100.
[58] M. Hillert and M. Jarl, A model for alloying in ferromagnetic metals, Calphad **2** (1978) 227-238.
[59] A. Dinsdale, SGTE data for pure elements, Calphad **15** (1991) 317-425.
[60] M. A. Turchanin, P. G. Agraval, and I. V. Nikolaenko, Thermodynamics of alloys and phase equilibria in the copper-iron system, J. Phase Equilib. **24** (2003) 307-319.

[61] W. Zhuang, Z.-Y. Qiao, S. Wei, and J. Shen, Thermodynamic evaluation of the Cu-R (R: Ce, Pr, Nd, Sm) binary systems, J. Phase Equilib. **17** (1996) 508-521.
[62] X. L. Chen, J. Wang, T. L. Chen, X. D. Lin, M. H. Rong, G. H.Rao, and H. Y. Zhou, Thermodynamic re-assessment of the Fe-Gd and Fe-Sm binary systems, Calphad **58** (2017) 151-159.
[63] PANDAT, CompuTherm LLC: https://computherm.com/ (accessed on 2022.12.21)
[64] Thermo-Calc, Thermo-Calc Software AB: https://thermocalc.com/ (accessed on 2022.12.21)
[65] S. Nishino and Y. Gohda, Structures of Sm-Cu intermetallics with Fe as subphase candidates in $SmFe_{12}$-based permanent magnets studied by first-principles thermodynamics, Jpn. J. Appl. Phys., in press.
[66] S. Idrissi, S. Ziti, H. Labrim, and L. Bahmad, Half-Metallicity and Magnetism in the Full Heusler Alloy Fe_2MnSn with $L2_1$ and XA Stability Ordering Phases, J. Low Temp. Phys. **202** (2021) 343–359.
[67] S. Idrissi, L. Bahmad, R. Khalladi, I. El Housni, N. El Mekkaoui, S. Mtougui, H. Labrim, and S. Ziti, Phase diagrams, electronic and magnetic properties of the quaternary Heusler alloy NbRhCrAl, Chinese J. Phys. **60** (2019) 549–563.
[68] S. Idrissi, H. Labrim, S. Ziti, and L. Bahmad, A DFT study of the equiatomic quaternary Heusler alloys ZnCdXMn (X=Pd, Ni or Pt), Solid State Commun. **331** (2021) 114292.